Evidence for Two Extremes of Ciliary Motor Response in a Single Swimming Microorganism

Ilyong Jung,[†] Thomas R. Powers,[†‡] and James M. Valles, Jr.[†*]
[†]Department of Physics and [‡]School of Engineering, Brown University, Providence, Rhode Island

ABSTRACT Because arrays of motile cilia drive fluids for a range of processes, the versatile mechano-chemical mechanism coordinating them has been under scrutiny. The protist *Paramecium* presents opportunities to compare how groups of cilia perform two distinct functions, swimming propulsion and nutrient uptake. We present how the body cilia responsible for propulsion and the oral-groove cilia responsible for nutrient uptake respond to changes in their mechanical environment accomplished by varying the fluid viscosity over a factor of 7. Analysis with a phenomenological model of trajectories of swimmers made neutrally buoyant with magnetic forces combined with high-speed imaging of ciliary beating reveal that the body cilia exert a nearly constant propulsive force primarily by reducing their beat frequency as viscosity increases. By contrast, the oral-groove cilia beat at a nearly constant frequency. The existence of two extremes of motor response in a unicellular organism prompts unique investigations of factors controlling ciliary beating.

INTRODUCTION

There are thousands of cilia covering *Paramecia* that beat to both propel and feed them (1). Two spatially contiguous groups accomplish these tasks. The cilia in the oral groove that leads toward the gullet control flows near the gullet (2). These flows provide nourishment while sampling the chemistry of the nearby environment. The cilia that cover the outermost surfaces largely control the swimming. In addition to propelling *Paramecia* along their nominal helical trajectories, these body cilia can beat to turn, reverse direction, or accelerate in response to environmental cues (1,3). It is remarkable that these two structurally similar groups, which share a common intracellular space, can effectively perform such disparate functions.

Here, we have investigated whether these groups of cilia can be differentiated by their so-called motor characteristics. A motor characteristic is the relation between the force exerted by and the speed at which a motor operates (4–9). For biological motors, the characteristic is dictated by a network of mechanical and chemical elements. In the case of *Paramecia*, this network includes elements that enable the body-cilia to respond to mechanical perturbations. For example, a jab to the posterior causes swimming acceleration, or a decrease in buoyancy causes greater upward propulsion (10,11). It seems likely that the oral groove and body-cilia networks have evolved to produce motor characteristics optimized for their different functions.

An established method for probing the characteristics of small biological motors is to observe their operation in media with a range of viscosities. This approach works well for systems operating in the low Reynold's number Stokes limit because the forces on the moving elements, which produce the load on the motor, are directly proportional to the viscosity η (4,7). It has been applied to ciliary systems operating in a variety of organisms (12–16). Information about *Paramecia* ciliary motor characteristics derived using this method, however, has been somewhat mixed. Pigon and Szarski (17), Tawada and Oosawa (18), and Yagi et al. (19) reported that the swimming speed decreases approximately inversely with viscosity implying a constant force-versus-speed propulsion motor characteristic. Sleigh (20) reported that the ciliary-beat frequency also decreased with viscosity, suggesting that the swimming speed decrease was directly related to slowing of the cilia. Subsequently, however, Machemer (21) showed that the ciliary-beat frequency varied significantly over the body. Moreover, he presented measurements showing that the oral groove cilia-beat frequency decreased only ~20% for a factor-of-10 change in viscosity. He presumed that the body cilia experienced a similarly small frequency decrease, implying that their ciliary motors operate at nearly constant speed.

We have combined high-speed, high magnification video investigations of ciliary motion with lower magnification studies of swimming trajectories and a phenomenological model to acquire a detailed picture of *Paramecia*'s ciliary motor characteristics. Uniquely, we have used the variation of the helical radius, helical pitch, and speed of the motion to infer how the speed and direction of the body-cilia-beating changes with viscosity. Our results, for $1 < \eta_w < 7$, where η_w is the viscosity normalized to water, recapitulate findings from the previous investigations like the slowing of *Paramecia*'s linear speed with increasing viscosity and the variation of ciliary-beat frequency over the body. In addition, we have found that the ciliary-beat frequency variation with viscosity depends on the region of the surface. In particular, the beat frequency in the oral groove barely

Submitted August 20, 2013, and accepted for publication November 15, 2013.

*Correspondence: james_valles_jr@brown.edu

Editor: Margaret Gardel.

0006-3495/14/01/0106/8 $2.00

http://dx.doi.org/10.1016/j.bpj.2013.11.3703

changes whereas the beat frequency in the mid-body region decreases almost inversely with viscosity.

We also found that the rotation rate of a swimming *Paramecium* decreases at nearly the same rate as the linear speed, indicating that the propelling torques have the same viscosity dependence as the propulsion force. Data analysis with a phenomenological model employing only a very few parameters implies that these swimming changes largely result from the mid-body cilia decreasing their beat speed without changing their beat angle. The model also shows that the oral-groove cilia beating contributes to the rotational motion of the swimmers. The results imply that the mid-body cilia have a constant force characteristic. This characteristic agrees well with contemporarily available numerical models of ciliary motion (22–24). The oral-groove cilia, on the other hand, exhibit a roughly constant speed motor characteristic. We believe that the observation of two such distinct motor characteristics in a single cell is unique. We point out that this finding suggests further *Paramecia* studies for insight into factors controlling ciliary motor response.

MATERIALS AND METHODS

Culturing *Paramecium caudatum*

Paramecium caudatum (Carolina Biological Supply, Burlington, NC) was cultured with its food, *Enterobacter aerogenes* (Carolina Biological Supply). At the stationary phase of their growth, they were collected by using their gravitaxis (25). The collected *Paramecia* were suspended in test solution containing 1 mM $CaCl_2$, 1 mM KCL, 0.1 mM $MgSO_4$, and 1.5 mM MOPS at PH ~7.2 and various concentrations of methylcellulose and magnetic impurities for at least 2 h before putting them in experimental chambers.

Viscous solution

We created viscous solutions by adding methylcellulose (Sigma Aldrich, St. Louis, MO) to test solution. We chose methylcellulose to make clear connections with previous experiments on *Paramecia* (18,21). Also, the density of the methylcellulose solutions are more comparable to water than, for example, Ficoll solutions of the same viscosity. The methylcellulose solutions were made in two steps: First, a high-concentration methylcellulose solution was made by mixing methylcellulose with test solution; second, the high concentration methylcellulose solution was diluted with test solution to produce a solution with the reduced η. The dilutions were done by inverting the mixing tubes ~10 times. Viscosities were measured at constant flow using glass capillary viscometers (Cannon Instrument, State College, PA). The experimental solutions had methylcellulose concentrations of 0, 0.2, 0.33, and 0.5% and η_w of 1.0, 2.3, 4.1, and 6.9, respectively. A cone and plate rheometer (model No. AR2000; TA Instruments, New Castle, DE) was used to determine the elastic modulus of a concentrated solution with $\eta_w = 7.9$. It was >25 times smaller than the viscous term at 10 Hz. At the methylcellulose concentration of 0.5%, the density of the solution was 0.2% larger than pure test solution. The molecular mass of the methylcellulose employed was 41 kDa, which corresponds to a radius of gyration of ~25 nm (26). The areal density of the cilia was ~1/(300 nm)^2. Thus, the radius of gyration is ~1/10th the spacing between cilia. At a concentration of 0.5%, the intermolecular spacing was ~25 nm. The solutions with enhanced magnetic susceptibilities for magnetic force buoyancy variation (MFBV) were made by doping (27,28) with a few millimolar of paramagnetic impurities (Gd-DTPA; Sigma Aldrich).

Swimming trajectory experimental setup

For trajectory measurements, populations of *Paramecia* swam in rectangular chambers of dimensions 2 × 16 × 16 mm (see Fig. 1). The chambers were formed with a frame made of Plexiglas (Rohm and Haas, Philadelphia, PA) sandwiched by two coverslips. The coverslips were sealed to the frame with VALAP (1:1:1, vaseline/lanolin/paraffin), which is nontoxic for microorganisms. A glass strip bisected the chamber to enable seeing both up- and down-swimmers concurrently. The *Paramecia*-containing solutions were carefully injected by a syringe through a hole in the chamber frame. The temperature of the swimming-chamber assembly was held to 23 ± 1°C by using a water-circulating bath. Swimming *Paramecia*, which were allowed to acclimate to the experimental chamber for at least 10 min, were recorded using a 90° side-view borescope (model No. 123008; ITI, Westfield, MA) and a charge-coupled device camera (XCD-SX 90; Sony, Tokyo, Japan) at 7.5 frames/s. A green LED array (TBL 1 × 1; Metaphase Technologies, Bensalem, PA) backlit the samples.

Magnetic force buoyancy variation

Swimming trajectory parameters were determined by observing *Paramecia* swimming under simulated neutral buoyancy conditions to eliminate sedimentation and gravikinetic effects (11,29). *Paramecia* were subjected to neutral buoyancy conditions using the method of MFBV. In this method, the chambers were placed in the bore of a resistive magnet at the National High Magnetic Field Laboratory (Tallahassee, FL). This made the *Paramecia* swim in an intense and inhomogeneous magnetic field (30) in solutions doped with paramagnetic impurities (Gd-DTPA; Sigma Aldrich) (27,28). The magnetic force exerted on a *Paramecium* and the solution makes the apparent weight magnetic-field-dependent, as

$$\frac{W}{W_{1g}} = \left(1 - \frac{\chi_P - \chi_S}{\rho_P - \rho_S}\frac{B}{g\mu_0}\frac{dB}{dz}\right), \qquad (1)$$

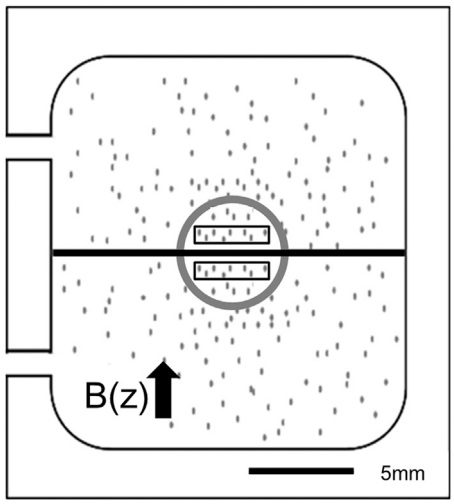

FIGURE 1 Experimental chamber. The small dots indicate *Paramecia*. The solid line in the middle of the chamber is a glass strip that separates the 2 × 16 × 16 mm chamber into two chambers. The fact that there are two chambers is not important for this work. (*Shaded circle* and *open box regions* inside the *circle*) Field of view and areas of interest, where swimming analysis was done, respectively. Note that two holes were needed to inject *Paramecia*.

where W is the apparent weight; ρ_P and ρ_S are the densities of the *Paramecia* ($_P$) and solution ($_S$); χ_P and χ_S are the magnetic susceptibilities of the *Paramecia* ($_P$) and solution ($_S$); z is the vertical coordinate; g is the acceleration of gravity; and μ_0 is the permeability of free space. The swimming chambers were placed in a maximum magnetic force region of a 31-Tesla maximum field resistive magnet at the National High Magnetic Field Laboratory. Adjusting the current in the magnet alters $B(dB/dz)$ to alter the apparent weight. Note that the apparent weight force can be inverted as well as augmented or reduced. Data presented here were obtained for *Paramecia* swimming with $W = 0$. To determine the correct magnetic field to levitate *Paramecia*, we immobilized *Paramecia* using 0.5 mM $NiCl_2$. After they were immobilized, we measured the magnetic field where $W = 0$ by increasing or decreasing the magnetic field until immobilized *Paramecia* stopped sedimenting or rising.

Image tracking

More than 50 trajectories were analyzed for each η. The tracks of the swimming trajectories were obtained and analyzed using IMAGE PRO ANALYZER 7.0 (Media Cybernetics, Rockville, MD). We set the rectangular area of interest at least 10 body lengths away from the Plexiglas frame (Rohm and Haas) and the cover-glass strip, as shown in Fig. 1. *Paramecia* that were very close to the top and the bottom cover glasses were filtered by focusing the borescope on the middle of the chamber. The depth of focus of the borescope was ~1 mm. The individual two-dimensional swimming tracks were fit to $x = R\sin(2\pi z/\lambda + \phi)$, where x, z, ϕ, R, and λ are the horizontal and vertical coordinates, a phase constant, amplitude, and wavelength, respectively. Note that the z axis points along the applied magnetic field, which is the direction along which the trajectories tended to align (30). Fits with $R^2_{\text{reduced}} < 0.9$ or of tracks shorter than one wavelength were discarded. Using the parameters describing the two-dimensional tracks, we obtained the angular frequency of the motion ω using $\omega = (2\pi/\lambda)(\Delta z/\Delta t)$ and the speed along the three-dimensional helical trajectories using $v = \omega\sqrt{R^2 + (\lambda/2\pi)^2}$ (31). The components of ω were obtained using

$$\omega^2 = \omega_\parallel^2 + \omega_\perp^2, \tag{2}$$

$$\frac{\omega_\parallel}{\omega_\perp} = \frac{\lambda}{2\pi R}. \tag{3}$$

Beating frequency measurement

For high-speed video measurements of ciliary motion, *Paramecia*-containing solutions were placed in drops sandwiched between coverslips separated by Parafilm sheets (Sigma-Aldrich) of ~125-μm thickness. This relatively constrained geometry caused their swimming trajectories to deviate from normal but seemed to exert little influence on their swimming speed. We inferred the beat frequencies by observing the periodic appearance of metachronal wave features in the form of crests or collective sweeps of groups of cilia at fixed positions along a *Paramecium*'s surface (see Movie S1, Movie S2, Movie S3, and Movie S4 in the Supporting Material). Examples of crests are indicated in Fig. 2 *a*. The period of time between crest appearances corresponds to the period of time between recovery strokes. The wavecrests appear sharper or more diffuse in the movies depending on the direction of the metachronal wave propagation or the location on the body. The samples were imaged using the phase contrast optics of an inverted light microscope (TE2000; Nikon, Tokyo, Japan) and recorded at 500 frames per second using a fast camera (Fastcam PCI R2; Photron USA, San Diego, CA) and its associated software (FASTCAM VIEWER; Photron USA). Frequencies of ciliary beating were determined by measuring the period of motion of groups of cilia at fixed positions on the body.

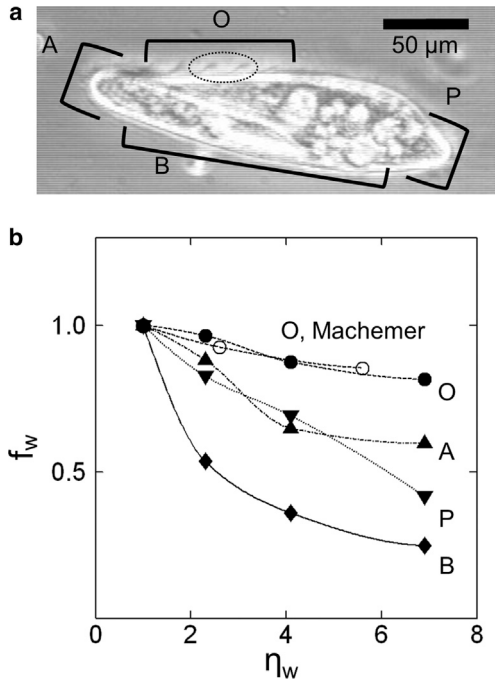

FIGURE 2 Viscosity dependence of ciliary beat frequencies. (*a*) Phase contrast image of a *Paramecium*. The brackets define four observation regions: *O*, oral groove; *A*, anterior; *B*, mid-body; and *P*, posterior. Examples of two metachronal wave crests can be seen within the dotted ellipse. The scale bar is 50 μm. (*b*) Ciliary-beat frequencies, f_w, measured in the four regions (*solid symbols*) normalized to their average value in standard test solution plotted versus η_w. Results obtained for the oral groove by Machemer (21) (*open circles*) are shown for comparison. (*Lines*) Guides to the eye.

RESULTS

High-speed imaging of ciliary motion

The surface of a *Paramecium* was divided into four regions (anterior, mid-body, oral groove, and posterior) for observations of ciliary motion (Fig. 2 *a*). We obtained the beat frequencies for *Paramecia* swimming at speeds comparable to their speeds far from walls. Consequently, we presumed that the beating frequencies obtained in the more constrained chambers were similar to those in the larger chambers. We measured the beating frequencies by noting the time between appearances of collective structures like the crests shown in Fig. 2 *a* at a fixed position on a *Paramecium* (see Movie S1, Movie S2, Movie S3, and Movie S4). The cilia forming these crests are executing their recovery stroke. The crest motion along the surface is a manifestation of the antiplectic metachronal wave associated with the coordination of the ciliary beating (32). As shown in Table 1, the frequency of ciliary beating varies over the surface at a fixed viscosity. It is highest in the oral groove and anterior regions and diminishes toward the posterior. This anterior-to-posterior gradient was noted previously (21). Fig. 2 *b* shows that the beat frequencies, f_w, normalized to their water values respond differently to increasing viscosity in the four regions. Here, and throughout, the w subscript denotes a

TABLE 1 Averaged ciliary beat frequencies in the four different regions from five measurements

η/η_w	Oral groove	Anterior	Body	Posterior
1.0	35.5 ± 3.1 Hz	34.5 ± 3.4 Hz	31.4 ± 8.3 Hz	15.2 ± 2.3 Hz
2.3	34.3 ± 1.0 Hz	30.4 ± 4.5 Hz	15.7 ± 2.1 Hz	12.6 ± 1.6 Hz
4.1	31.0 ± 3.4 Hz	22.4 ± 4.3 Hz	11.3 ± 1.6 Hz	10.5 ± 2.0 Hz
6.9	29.0 ± 3.6 Hz	20.6 ± 4.8 Hz	7.8 ± 1.0 Hz	6.3 ± 1.3 Hz

quantity normalized by its value for water. The body-ciliary-beat frequency changes the most, decreasing by a factor of 4 for the factor-of-7 change in viscosity. In sharpest contrast, the oral-groove frequency changes little, decreasing by only 20%. The anterior and posterior frequencies show intermediate behavior, with the posterior frequency diminishing more.

These differences indicate that the ciliary motor regulation varies over the surface, ranging between two extremes. The oral-groove cilia are regulated to beat at a nearly constant frequency. The mid-body cilia, on the other hand, appear regulated to beat with

$$\text{Viscosity} \times \text{Frequency} \cong \text{Constant}.$$

Because the drag forces in the Stokes flow regime are proportional to

$$\text{Viscosity} \times \text{Speed},$$

this dependence suggests nearly constant force regulation. In the next section, we present an analysis of swimming trajectories that strongly supports this assertion.

Swimming trajectory investigations

To characterize the ciliary motor for propulsion, we performed a series of measurements of *Paramecia* swimming trajectories in different viscosities. This approach follows that of a number of experiments (4–8) on bacteria that have varied viscosity to obtain force-velocity curves of their flagellar motors that, in turn, have been used to test models of the motors. The relatively straightforward separation of the part of the organism responsible for propulsion—the flagellum—from the part of the bacterium that experiences drag alone—the body—simplifies that analysis (6,33). Correspondingly, some experiments characterized bacterial flagellar motors by measuring the rotation rates of the flagella of bacteria with their heads fixed to a surface (34). Others used simultaneous measurements of the head rotation rate and swimming speed with a model of force and torque balance to calculate the motor characteristic (8,35,36). For microorganisms like *Paramecium caudatum*, propulsion results from the coordinated beating of thousands of cilia that uniformly cover their body. The propulsion and drag both depend on the details of the beating of the individual cilia as well as the coordination among cilia and the body shape (1).

Machemer's detailed characterization (21) of ciliary beating as a function of viscosity showed that the geometry and rate of the individual beating and the metachronal coordination change systematically. The specifics of how to translate Machemer's ciliary observations (21) to the propulsive forces they generate, however, represent a significant challenge in fluid dynamics modeling. Extensions of contemporary numerical theoretical models that predict how effectively a small number of cilia and flagella propel themselves in fluids of varying viscosity are required (14,22–24,37–39). By measuring the trajectories, we are able to determine the net forces and torques exerted by the cilia that are responsible for their motion. This approach allows us to obtain the motor characteristics of the propulsion system as a whole.

A neutrally buoyant *Paramecium* normally swims along a helical trajectory with its body aligned tangent to its path and its oral groove facing the axis of the helix (Fig. 3, *a* and *b*) (40–42). This motion decomposes into a linear translation characterized by a speed v and a precession about an axis parallel to the axis of the helix (43). The precession angular velocity has components along two orthogonal body axes, $\omega_{||}$ and $\omega_{\perp}$. Experimentally, $\omega_{||}$ and $\omega_{\perp}$ are calculated from measurements of the maximum speed and the wavelength and the amplitude of the sinusoidal form of the two-dimensional projection of the helix. The decomposition of the motion only works in the absence of sedimentation because the long axis of a sedimenting swimmer does not align tangent to the helix. We have employed the method of MFBV (11,44) to make the *Paramecia* neutrally buoyant. This technique employs paramagnetic impurities and magnetic force rather than fluid density adjustment to alter the buoyancy.

At each viscosity, >50 swimming trajectories were analyzed for the linear speed v and two angular speeds, $\omega_{||}$ and $\omega_{\perp}$. The average values of all three speeds decrease monotonically with viscosity as shown in Fig. 3, *c–e*. The corresponding helix wavelengths range from 500–1000 μm and helix radii range from 40–150 μm (see Movie S1, Movie S2, Movie S3, and Movie S4) (45,46). In addition, the standard deviations of the speed distributions, indicated by the bars on the data points, decrease monotonically at roughly the same rate as the speeds. This result gives us confidence that the changes in medium viscosity influence swimmers throughout the speed distribution similarly. At this point, it is important to establish whether this is a purely viscous response, because methylcellulose solutions are known to exhibit visco-elastic effects at high concentrations. To check, we measured the speed as a function of viscosity of *Paramecia* in Ficoll solutions that are known to be Newtonian. The nearly identical $v(\eta)$ characteristics (see Fig. 3 *c*, and see Fig. S1 in the Supporting Material) imply that non-Newtonian effects exert a negligible influence on the swimming. Further, an estimate of the Reynolds number for the lowest viscosity and highest speeds gives $Re < 0.1$ (32), which implies that inertial effects on the flows are small.

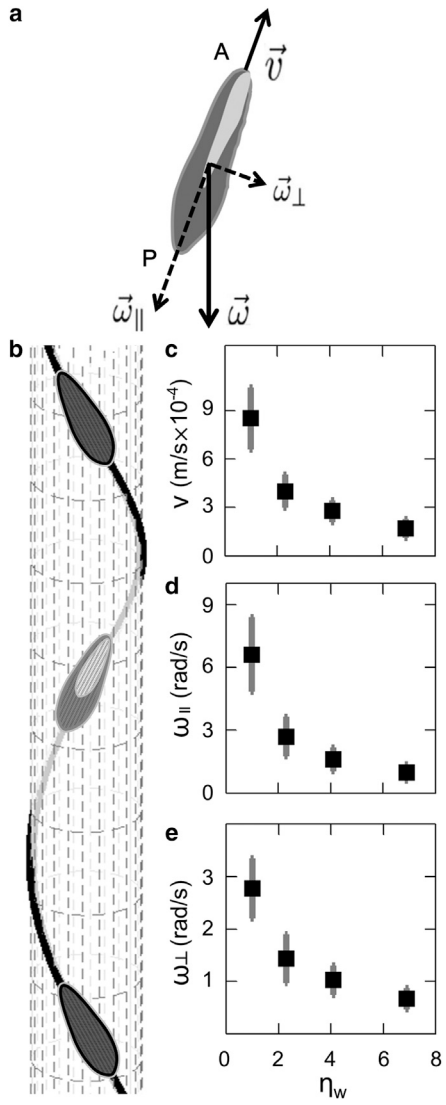

FIGURE 3 Viscosity dependence of swimming trajectory parameters. (a) Sketch of a *Paramecium* indicating the translational velocity vector $\vec{v}$ and the rotational velocity vector $\vec{\omega}$ that produce its motion along a left-handed helical trajectory, as shown in panel *b*. The labels *A* and *P* denote the anterior and posterior regions, respectively. (*Light-shaded area*) Oral groove. (*c–e*) Averages of v, $\omega_{||}$, and $\omega_\perp$, respectively, derived from analysis of >50 trajectories at each viscosity. (*Bars*) Standard deviation of the populations.

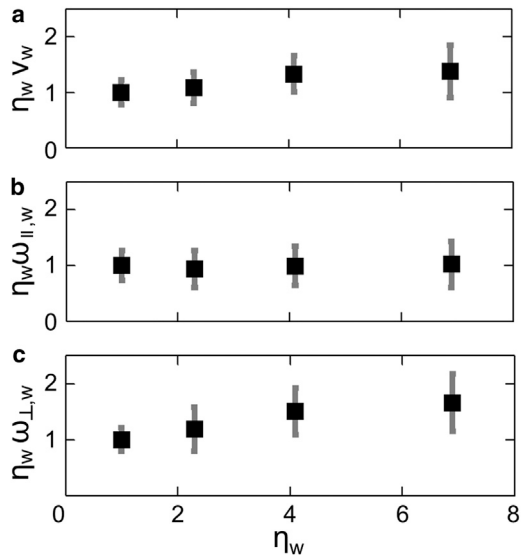

FIGURE 4 Viscosity dependence of propulsive forces and torques. (*a–c*) Products of the viscosity with each of the rates shown in Fig. 3. (*Bars*) Standard deviation of the populations.

In this Stokes regime and under conditions of neutral buoyancy, the propulsion forces and torques are proportional to these speeds and the viscosity. Provided the body is axisymmetric, they are decoupled. We plot the normalized propulsion force $p_w = \eta_w v_w$ and torques, $\tau_{||,w} = \eta_w \omega_{||,w}$ and $\tau_{\perp,w} = \eta_w \omega_{\perp,w}$, as a function of η_w in Fig. 4, *a–c*. All three exhibit a weak dependence on viscosity. For example, $\tau_{\perp,w}$, which changes the most, only increases by ~60% for the factor-of-7 change in viscosity. The propulsive force varies $< \pm 30\%$, which implies that $v \sim \eta^{-1}$ as found earlier (17,18). In other words, the ciliary motors driving translation and rotation exhibit nearly constant force (p,$\tau_{||}$,$\tau_\perp$) versus speed (v,$\omega_{||}$,$\omega_\perp$) characteristics.

The similarity of the propulsive force and torques motor characteristics provides insight into how the forces exerted by the cilia vary over the body. Each motor characteristic depends differently on the spatial distribution of forces as well as the variations in force magnitudes and directions. The propulsion force depends on the vector sum of the forces exerted by the different regions of the surface but does not depend on the spatial distribution of the forces. The torques, on the other hand, depend on the spatial force distribution because it determines the moment arms through which the forces act and depend on different components of the forces. For example, $\tau_\perp$ is more strongly influenced by forces close to the anterior and posterior regions than the cilia in the mid-body region whereas the opposite holds true for $\tau_{||}$. Moreover, forces directed from A to P exert the primary influence on $\tau_\perp$ whereas forces in the azimuthal direction exert the primary influence on $\tau_{||}$. Thus, a simple conclusion from the data is that the magnitudes and directions of the forces exerted by the different regions do not change with viscosity.

Phenomenological model analysis of ciliary-based propulsion

We use a phenomenological model to relate the force exerted by the ciliary beating of an average region on the body and in the oral groove to the trajectory parameters. One of the unique features of this model is that it predicts correlations between trajectory parameters that provide an internal consistency check. The presumption that an average region provides a meaningful description is supported by the

discussion above as well as the observations of the highly coordinated metachronal ciliary-beating waves that travel coherently along the body (21). It has been invoked in previous qualitative descriptions of the relation between ciliary activity and propulsion (40) and other quantitative analyses of gravity-dependent swimming of *Paramecia* (41,42). Following Machemer (41) and Mogami and Baba (42), we characterize the time-averaged force exerted by an average region using two parameters: a speed u_B, which could reflect the average speed of the cilia relative to the cell body; and an angle θ, measured relative to a vector pointing from P to A along the local longitude. This angle could reflect the direction of the trajectory of the cilia tips during the power stroke. We also include the influence of the oral-groove cilia on the rotation of the swimmers as qualitatively described by Jennings (40). The oral-groove cilia are presumed to beat in a fixed direction with a distinct speed u_O. This beating contributes to the torque $\tau_\perp$ that gives rise to $\omega_\perp$, but not to the propulsion.

Thus, we write the propulsive force and the two torques, which are proportional to η, as

$$p = -A\eta u_B \cos\theta, \tag{4}$$

$$\tau_\parallel = -N_\parallel \eta u_B \sin\theta, \tag{5}$$

$$\tau_\perp = -N_\perp \eta u_B \cos\theta + M\eta u_O. \tag{6}$$

The constants A, $N_\parallel$, $N_\perp$, and M increase with the number, length, and density of the cilia and on the size and shape of the body. The N and M constants are also proportional to the effective moment arm through which the forces act. $N_\perp$ originates from the asymmetry in the body cilia distribution due to the existence of the oral groove. Note that A has units of length, and M and the N constants have units of length-squared. All are taken to be positive.

To relate the force and torques to the kinematics, we assume low Reynold's number dynamics and that the body has the symmetric shape of a prolate ellipsoid so that there is no coupling between the linear and rotational velocities in the resistance matrix (37). The propulsive force p balances the drag force, leading to speed $v = p/(\eta C_L)$, where C_L is the body's longitudinal drag coefficient. The torques lead to rotations $\omega_\parallel = \tau_\parallel/(\eta\gamma_\parallel)$ and $\omega_\perp = \tau_\perp/(\eta\gamma_\perp)$, where $\gamma_\parallel$ and $\gamma_\perp$ are the rotational drag coefficients. Thus,

$$v = -\frac{A}{C_L} u_B \cos\theta, \tag{7}$$

$$\omega_\parallel = -\frac{N_\parallel}{\gamma_\parallel} u_B \sin\theta, \tag{8}$$

$$\omega_\perp = -\frac{N_\perp}{\gamma_\perp} u_B \cos\theta + \frac{M}{\gamma_\perp} u_O. \tag{9}$$

We can isolate the θ-dependence with the ratio

$$\frac{\omega_\parallel}{v} = G_1 \tan\theta, \tag{10}$$

where $G_1 = (N_\parallel/\gamma_\parallel)(C_L/A)$ depends on the number of body cilia and the shape of a *Paramecium*. This model also predicts a correlation between v and $\omega_\perp$, according to Eqs. 7 and 9, in the form

$$\omega_\perp = G_2 v + G_3 u_O, \tag{11}$$

where $G_2 = (N_\perp/\gamma_\perp)(C_L/A)$ and $G_3 = M/\gamma_\perp$ are constants depending on the number of cilia and the shape of a *Paramecium*. They are independent of η.

With the above relations in hand, we turn to the swimming data. The decrease in v with η implies that $u_B \cos\theta$ decreases with η, presuming A and C_L are independent of viscosity. To determine whether this decrease results from changes in either u_B or θ or both, we plotted $\omega_\parallel/v$ as a function of η_w in Fig. 5 *a* to compare to Eq. 10. The plots show $\omega_\parallel/v$, which corresponds to $\tan\theta$ decreasing by ~30%. This behavior qualitatively agrees with Machemer's observation of a clockwise rotation of the power-stroke direction with increasing viscosity (21). Using $\theta = \pi/6$ at $\eta_w = 1$, corresponding to the power-stroke direction measured by Machemer (21), we estimate θ at $\eta_w = 6.9$ to be 22°. This corresponds to only a 7% increase in $\cos\theta$.

Consequently, the large decrease in v with η corresponds to a similar decrease in u_B. The dependence of $\omega_\perp$ on v shown in Fig. 5 *b* supports the presumption that the constants depending on the spatial distribution of beating cilia, like A, are independent of viscosity. The value $\omega_\perp$ grows nearly linearly with v, implying that G_2 and $G_3 u_O$ (see Eq. 11) depend very little on η. In addition, the small intercept indicates that the oral-groove beating contributes only ~10% to the rotation at normal viscosity and ~30% at $\eta_w = 6.9$. This contribution is small enough that the ~15% decrease in oral-groove beat frequency is consistent with

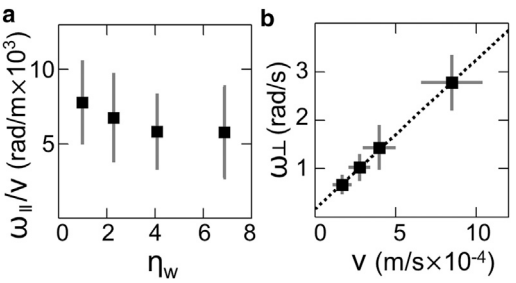

FIGURE 5 Insights from the phenomenological model. (*a*) Plot of $\omega_\parallel/v$ versus η_w to compare to Eq. 10. This ratio is proportional to $\tan\theta$, where θ gives the direction of the force exerted by the average patch of cilia. (*b*) $\omega_\perp$ versus v to compare to Eq. 11 at different viscosities. The intercept gives the oral-groove cilia contribution to the torque producing $\omega_\perp$. The line is a fit that tests the expected linear dependence of $\omega_\perp$ on v. (*Bars*) Standard deviation of the populations.

u_O being constant in this viscosity range. To summarize, the analysis with this phenomenological model indicates that the decrease in v, $\omega_{||}$, and $\omega_{\perp}$ with η results primarily from a decrease in u_B. In addition, the spatial distribution of beating cilia embodied in the constants, A, N, and M does not depend on viscosity. We suggest that this model may be helpful for interpreting swimming trajectory changes induced by other parameters like temperature (18) and gravity (11,29,47,48).

DISCUSSION

The phenomenological model analysis implies that the mid-body cilia produce a constant propulsion force by reducing their beating speed with viscosity. This result agrees well with the direct measurements of the mid-body cilia-beat frequency, which show it to decrease nearly inversely proportional to viscosity (Fig. 2 *b*). It contrasts sharply with the oral-groove beat frequency, which barely changes.

It is important to note that neither of these motor characteristics is anomalous. Like the body-cilia in *Paramecia*, the beat frequency of the lateral cilia in the mussel *Mytilus edulis* rapidly changes by ~40% as viscosity changes from 1 to 1.7 cP (16). In contrast, like the oral-groove cilia, the beat frequencies of cilia in rabbit trachea (12), *Planaria* (13), and frog esophagus (14) change only by tens of percent for many-fold increases in viscosity above the water value. For example, rabbit trachea reduces its beat rate by only 30% as viscosity increases from 1 to 15 cP. What is new, to our knowledge, in our results is the occurrence of the two extremes of motor behaviors in a single cell.

Models of ciliary beating (22–24) produce motor characteristics like the mid-body cilia. These models include the elastic properties of the cilia, the internal force generation by molecular motors, and the interaction of the cilia with their surrounding fluid. They predict the shape of the stroke, the coordination among cilia, and the rate of beating. Nearly uniformly, they show that the frequency of beating decreases whereas the geometry of the beating varies little with viscosity. This behavior implies that the effective propulsive force $\propto \eta_f$. As shown in Fig. 6 *a*, the model predictions more closely follow the viscosity dependence of the mid-body ciliary-beat frequency and the propulsion force than the oral-groove cilia. Fig. 6 *b* translates this comparison into the motor characteristics. The force-versus-speed motor characteristics are horizontal for the ciliary swimming motors and the models but vertical for the oral-groove ciliary motor.

Whether simple modifications of the models will enable them to capture the oral-groove constant speed characteristics requires further work. Experiments on *Paramecia* that compare the responses of the mid-body and oral-groove cilia to chemical and mechanical perturbations have the potential to give insight into the factors that differentiate their motors. The open architecture of cortical sheet preparations like those used in recent studies of dynein and cyclic AMP interactions involved in ciliary beating (49) may be particularly attractive for such investigations.

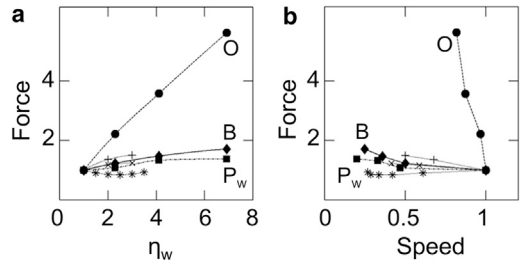

FIGURE 6 Comparisons of motor characteristics. Propulsive force, p_w, from these experiments and force predictions based on the measured beat frequencies, mid-body, *B*, and oral groove, *O*, shown in Fig. 2 *b*, and numerical model calculations (+ (22), × (23), and * (24) of beat frequencies). The forces are the product of the viscosity and the rate (i.e., speed or frequency). (*a*) Forces as a function of viscosity. (*b*) Forces as a function of rates. All forces and rates are normalized to their values in water. (*Lines*) Guides to the eye.

SUPPORTING MATERIAL

One figure and eight movies are available at http://www.biophysj.org/biophysj/supplemental/S0006-3495(13)04962-X.

We are grateful for discussions with Jay Tang, Saverio Spagnolie, Kenny Breuer, and Guanglai Li. We appreciate Jay Tang's help with the use of his fast camera microscopy setup and Anubhav Tripathi's assistance with the measurements of the properties of methylcellulose solutions.

This work was supported by National Science Foundation grant No. PHY0750360 and at the National High Magnetic Field Laboratory by National Science Foundation grant No. DMR-0084173. T.R.P. thanks the Aspen Center for Physics, which is supported by National Science Foundation grant Nos. PHY-1066293 and CBET-0854108.

REFERENCES

1. Wichterman, R. 1986. The Biology of *Paramecium*. Plenum Press, New York.
2. van Wagtendonk, W. J. 1974. *Paramecium*: A Current Survey. Elsevier Scientific, New York.
3. Hamel, A., C. Fisch, …, C. N. Baroud. 2011. Transitions between three swimming gaits in *Paramecium* escape. *Proc. Natl. Acad. Sci. USA*. 108:7290–7295.
4. Hill, D. B., V. Swaminathan, …, R. Superfine. 2010. Force generation and dynamics of individual cilia under external loading. *Biophys. J.* 98:57–66.
5. Li, G., J. Bensson, …, Y. V. Brun. 2011. Accumulation of swimming bacteria near a solid surface. *Phys. Rev. E Stat. Nonlin. Soft Matter Phys.* 84:041932.
6. Li, G., and J. X. Tang. 2006. Low flagellar motor torque and high swimming efficiency of *Caulobacter crescentus* swarmer cells. *Biophys. J.* 91:2726–2734.
7. Chen, X., and H. C. Berg. 2000. Torque-speed relationship of the flagellar rotary motor of *Escherichia coli*. *Biophys. J.* 78:1036–1041.
8. Sowa, Y., H. Hotta, …, A. Ishijima. 2003. Torque-speed relationship of the Na^+-driven flagellar motor of *Vibrio alginolyticus*. *J. Mol. Biol.* 327:1043–1051.

9. Ryu, W. S., R. M. Berry, and H. C. Berg. 2000. Torque-generating units of the flagellar motor of *Escherichia coli* have a high duty ratio. *Nature.* 403:444–447.
10. Machemer, H. 1974. Frequency and directional responses of cilia to membrane potential changes in *Paramecium*. *J. Comp. Physiol. A Neuroethol. Sens. Neural Behav. Physiol.* 92:293–316.
11. Guevorkian, K., and J. M. Valles, Jr. 2006. Swimming *Paramecium* in magnetically simulated enhanced, reduced, and inverted gravity environments. *Proc. Natl. Acad. Sci. USA.* 103:13051–13056.
12. Johnson, N. T., M. Villalón, …, P. Verdugo. 1991. Autoregulation of beat frequency in respiratory ciliated cells. Demonstration by viscous loading. *Am. Rev. Respir. Dis.* 144:1091–1094.
13. Rompolas, P., R. S. Patel-King, and S. M. King. 2010. An outer arm dynein conformational switch is required for metachronal synchrony of motile cilia in *Planaria*. *Mol. Biol. Cell.* 21:3669–3679.
14. Gheber, L., A. Korngreen, and Z. Priel. 1998. Effect of viscosity on metachrony in mucus propelling cilia. *Cell Motil. Cytoskeleton.* 39: 9–20.
15. O'Callaghan, C. L., K. Sikand, …, R. A. Hirst. 2008. The effect of viscous loading on brain ependymal cilia. *Neurosci. Lett.* 439:56–60.
16. Larsen, P. S., and H. U. Riisgård. 2009. Viscosity and not biological mechanisms often controls the effects of temperature on ciliary activity and swimming velocity of small aquatic organisms. *J. Exp. Mar. Biol. Ecol.* 381:67–73.
17. Pigon, A., and H. Szarski. 1955. The velocity of the ciliary movement and the force of the ciliary beat in *Paramecium caudatum*. *Bull. Polish Acad. Sci.* 3:99–102.
18. Tawada, K., and F. Oosawa. 1972. Responses of *Paramecium* to temperature change. *J. Protozool.* 19:53–57.
19. Yagi, T., I. Minoura, …, R. Kamiya. 2005. An axonemal dynein particularly important for flagellar movement at high viscosity. Implications from a new *Chlamydomonas* mutant deficient in the dynein heavy chain gene DHC9. *J. Biol. Chem.* 280:41412–41420.
20. Sleigh, M. A. 1962. The Biology of Cilia and Flagella. Pergamon Press, New York.
21. Machemer, H. 1972. Ciliary activity and the origin of metachrony in *Paramecium*: effects of increased viscosity. *J. Exp. Biol.* 57:239–259.
22. Yang, X., R. H. Dillon, and L. J. Fauci. 2008. An integrative computational model of multiciliary beating. *Bull. Math. Biol.* 70:1192–1215.
23. Gueron, S., and K. Levit-Gurevich. 1998. Computation of the internal forces in cilia: application to ciliary motion, the effects of viscosity, and cilia interactions. *Biophys. J.* 74:1658–1676.
24. Guirao, B., and J. F. Joanny. 2007. Spontaneous creation of macroscopic flow and metachronal waves in an array of cilia. *Biophys. J.* 92:1900–1917.
25. Roberts, A. M. 2010. The mechanics of gravitaxis in *Paramecium*. *J. Exp. Biol.* 213:4158–4162.
26. Funami, T., Y. Kataoka, …, K. Nishinari. 2007. Thermal aggregation of methylcellulose with different molecular weights. *Food Hydrocoll.* 21:46–58.
27. Winkleman, A., K. L. Gudiksen, …, M. Prentiss. 2004. A magnetic trap for living cells suspended in a paramagnetic buffer. *Appl. Phys. Lett.* 85:2411.
28. Weinmann, H. J., R. C. Brasch, …, G. E. Wesbey. 1984. Characteristics of gadolinium-DTPA complex: a potential NMR contrast agent. *Am. J. Roentgenol.* 142:619–624.
29. Machemer, H., S. Machemer-Röhnisch, …, K. Takahashi. 1991. Gravikinesis in *Paramecium*: theory and isolation of a physiological response to the natural gravity vector. *J. Comp. Physiol. A Neuroethol. Sens. Neural Behav. Physiol.* 168:1–12.
30. Guevorkian, K., and J. M. Valles, Jr. 2006. Aligning *Paramecium caudatum* with static magnetic fields. *Biophys. J.* 90:3004–3011.
31. Crenshaw, H. C. 2006. Orientation by helical motion—1. Kinematics of the helical motion of organisms with up to six degrees of freedom. *Bull. Math. Biol.* 55:197–212.
32. Childress, S. 1981. Mechanics of Swimming and Flying. Cambridge University Press, London, UK.
33. Chattopadhyay, S., R. Moldovan, …, X. L. Wu. 2006. Swimming efficiency of bacterium *Escherichia coli*. *Proc. Natl. Acad. Sci. USA.* 103:13712–13717.
34. Berg, H. C. 2003. The rotary motor of bacterial flagella. *Annu. Rev. Biochem.* 72:19–54.
35. Magariyama, Y., and S. Kudo. 2002. A mathematical explanation of an increase in bacterial swimming speed with viscosity in linear-polymer solutions. *Biophys. J.* 83:733–739.
36. Magariyama, Y., S. Sugiyama, …, S. Kudo. 1995. Simultaneous measurement of bacterial flagellar rotation rate and swimming speed. *Biophys. J.* 69:2154–2162.
37. Lauga, E., and T. R. Powers. 2009. The hydrodynamics of swimming microorganisms. *Rep. Prog. Phys.* 72:096601.
38. Smith, D. J., E. A. Gaffney, and J. R. Blake. 2009. Mathematical modeling of cilia-driven transport of biological fluids. *Proc. Roy. Soc. A Math. Phys. Eng. Sci.* 465:2417–2439.
39. Fu, H. C., T. R. Powers, and C. W. Wolgemuth. 2007. Theory of swimming filaments in viscoelastic media. *Phys. Rev. Lett.* 99:258101.
40. Jennings, H. S. 1906. Behavior of the Lower Organisms. Columbia University Press, New York.
41. Machemer, H. 1996. A theory of gravikinesis in *Paramecium*. *Adv. Space Res.* 17:11–20.
42. Mogami, Y., and S. A. Baba. 1998. Super-helix model: a physiological model for gravitaxis of *Paramecium*. *Adv. Space Res.* 21:1291–1300.
43. Crenshaw, H. C. 1989. Kinematics of helical motion of microorganisms capable of motion with four degrees of freedom. *Biophys. J.* 56:1029–1035.
44. Guevorkian, K., and J. M. Valles, Jr. 2004. Varying the effective buoyancy of cells using magnetic force. *Appl. Phys. Lett.* 84:4863.
45. Guevorkian, K. 2006. Experimental studies of protozoan response to intense magnetic fields and forces. Ph.D. thesis, Brown University, Providence, RI.
46. Jana, S., S. H. Um, and S. Jung. 2012. *Paramecium* swimming in a capillary tube. *Phys. Fluids.* 24:041901.
47. Hemmersbach, R., and R. Bräucker. 2002. Gravity-related behavior in ciliates and flagellates. *Adv. Space Biol. Med.* 8:59–75.
48. Bräucker, R., and R. Hemmersbach. 2002. Ciliates as model systems for cellular graviperception. *J. Gravit. Physiol.* 9:249–252.
49. Kutomi, O., M. Hori, …, M. Noguchi. 2012. Outer dynein arm light chain 1 is essential for controlling the ciliary response to cyclic AMP in *Paramecium tetraurelia*. *Eukaryot. Cell.* 11:645–653.